

Robust propagating in-gap modes due to spin-orbit domain walls in graphene

Jean-Baptiste Touchais, Pascal Simon, and Andrej Mesaros*

Université Paris-Saclay, CNRS, Laboratoire de Physique des Solides, 91405, Orsay, France

(Dated: July 22, 2021)

Recent experimental progress in designing electronic states in layered heterostructures raises questions about inducing topological states in inhomogeneous systems. In particular, it has become clear that there is a delicate interplay of multiple spin-orbit terms induced in graphene on incommensurate transition metal dichalcogenide substrates, so that nano- to mesoscopic domains of different spin-orbit and mass values may form. We therefore investigate various types of domain walls in graphene looking for robust propagating electronic states, first by finding the states via analytical and topological arguments in the low-energy theory, and then studying their robustness to symmetry breaking and lattice backscattering effects in a tight-binding model. Surprisingly, we find that a sign-changing domain wall in Valley-Zeeman (VZ) spin-orbit coupling binds two robust Kramers pairs within the bulkgap opened due to a simultaneous presence of Rashba (R) coupling. We show the relation of these modes to a domain wall in gating of bilayer graphene. In a contrasting example, a sign-changing Kane-Mele (KM) spin-orbit coupling domain wall between two domains in the topological insulator (TI) phase, equivalent to two copies of a TI edge, has two pairs of helical modes that are stable to intervalley scattering, but not stable to breaking S_z symmetry, e.g., by a Rashba term. Nevertheless, there are also higher excited modes on a smooth KM domain wall which mimic Landau-levels of free spinless graphene. We also introduce a domain wall by rotating the spin direction of the Kane-Mele term in a spiral, and analytically explain the closing bulkgap and the lack of in-gap modes. We discuss the possible spectroscopic and transport signatures in heterostructures.

I. INTRODUCTION

Amid an explosion of research into van der Waals materials during this decade, graphene-based platforms remain central for discovery and design of topological states of matter. Today’s promising platforms are essentially tied to inhomogeneities in real space: one pathway is based on inducing spin-orbit coupling (SOC) in graphene by proximity to other crystals[1–3], leading to incommensurability effects; in another pathway, twisted multilayers may exploit domain structure to induce new electronic states, as observed in twisted bilayer graphene[4–7]; finally, one considers devices and heterostructures with purposefully designed variation of order parameters and external fields in real space. Therefore, understanding the electronic modes due to some spatial variations within multiple coupling parameters rises both fundamental and practical questions. In particular, SOC parameters remain in focus regarding design of topological states, especially since it became clear that multiple competing SOC terms are induced in proximitized graphene[2, 3, 8–10].

A special type of electronic states designed for spin- and valleytronics involve creating one-dimensional channels, which can essentially be understood as domain walls (DW) in a certain coupling parameter. One of the first proposals for topological channels was due to a gating DW in bilayer graphene[11], which was later connected to a DW in stacking order[12], leading to experimental observation of the one-dimensional modes[13]. Further

DWs in Dirac mass parameter yielded valley-polarized modes[14, 15]. Alternative DWs using strain field as the parameter were proposed[16, 17], while multilayer systems allow for even more coupling parameters[7, 18–20]. A unifying viewpoint of one-dimensional topological modes as DW modes is also exemplified in the unexpected robustness to magnetic field of quantum spin Hall (QSH) helical edge states that was understood from a DW between a QSH and a quantum Hall domain[21]. Understanding DWs in presence of multiple parameters is crucial, as becomes clear in the recent finding that QSH edge modes may be transformed or supplemented by spin- or valley-polarized modes as one changes the dominant SOC parameter[22, 23], however the treatment of non-randomly varying SOC parameters in this context remains scarce[24, 25].

A challenge in theoretically describing the nature and stability of induced electronic modes such as one-dimensional DW modes, is adapting topological methods to inhomogeneous situations. One may treat spatial coordinates classically at long distances from a topological defect, and consider the resulting band topology due to discrete symmetries[26, 27]. One may also use real-space expressions that give a local indication of non-trivial topology[28]. Nevertheless, a precise “bulk-defect” correspondence in this case remains quite abstract, invoking that generalized bulk topological numbers[29, 30] must cause some DW modes[31, 32]. More recently, the notion of using topological numbers associated to local information in parameter space[11, 33] resurfaced in the form of a spectral flow theorem (SFT),[34, 35] which is an exact statement about topologically protected quantum modes due to spatially varying parameters, based on local information near degeneracies in an auxiliary matrix

* andrej.mesaros@universite-paris-saclay.fr

operator. The SFT can therefore be a powerful tool to explicitly derive topological modes from Chern numbers, keeping track of symmetry through quantum numbers.

Here we study various domain walls in graphene with Kane-Mele (KM), valley-Zeeman (VZ) and Rashba (R) spin-orbit couplings, as well as Dirac mass, identifying topologically protected states using the spectral flow theorem, and confirming their robustness against intervalley scattering on lattice and against breaking spin symmetries. A summary of found modes for certain types of DWs is in Table I. One of our main findings is that a DW in VZ SOC in presence of arbitrary constant R SOC hosts two robust propagating valley-polarized Kramers pairs, derived from a Chern number $|C| = 2$. This is in contrast to previously identified graphene edge states due to VZ SOC that are fragile to lattice termination and coupling strength, and were connected to a valley-Chern number $|C| = 1$.[8, 22, 36] Interestingly our VZ DW modes are mapped exactly onto modes of a DW between two gated regions in spinless bilayer graphene[37]. Since proximitized graphene has been shown to acquire spatially-dependent SOC of all three types, where VZ is considerable, we expect that such modes may contribute to spectroscopic and transport properties. Another finding is that along the interface with two copies of QSH edge states, equivalent to a DW with opposite signs of KM SOC in two domains, the double Kramers pair of edge modes is robust to lattice effects and can only be gapped by breaking spin S_z conservation, e.g., by R SOC (assuming time reversal symmetry). A DW smooth on the nanoscale also hosts gapped excited modes inside the bulkgap[38], with the same spectrum as Landau levels of spinless graphene under effective magnetic field inversely proportional to the DW width. Consequently, a spatially varying KM SOC might host an in-gap tower of propagating modes which could be tuned by changing the spatial variation lengthscale and/or the strength of Rashba SOC.

The paper is organized as follows: In Section II we introduce the application of the SFT to find topologically protected modes in examples of continuum Dirac electrons of graphene combining KM SOC and Dirac mass term, and then proceed to include VZ and R SOC. The mapping to bilayer graphene is included here. In Section III we build tight-binding models to investigate the robustness of modes by varying DW profile between smooth and sharp on the lattice lengthscale. We also combine multiple couplings. In Section IV we return to the continuum theory of a sign-changing KM DW and map it to Landau levels of graphene. In Section V we consider a DW in which the KM SOC vector spirals and show it does not host propagating modes but instead map to a vector potential that closes the bulkgap as the spiral winding increases. We finish with a discussion including potential impact on experiments, and an outlook.

II. SMOOTH DOMAIN WALLS IN THE CONTINUUM

We start by considering the low-energy continuum Dirac theory for graphene with a smooth domain wall in a coupling parameter. We use a spectral flow theorem to identify topologically protected electron modes propagating along the DW between two gapped domains, and we discuss the protection of these modes.

Our model of a smooth domain wall in the continuum limit takes the form

$$H = \tau_z \sigma_x (-i\partial_x) + k_y \sigma_y + m(x) \sigma_z + \lambda_{KM}(x) \tau_z \sigma_z s_z + \lambda_{VZ}(x) \tau_z s_z + \lambda_R(x) (\tau_z \sigma_x s_y - \sigma_y s_x), \quad (1)$$

where we assume translational invariance along the domain wall in y direction (any direction is equivalent in the low-energy theory), the m , λ_{KM} , λ_{VZ} and λ_R are the Dirac mass, Kane-Mele spin orbit (KM), valley-Zeeman spin-orbit (VZ) and Rashba spin-orbit (R) couplings, respectively, and the Pauli matrices τ_i , σ_i , s_i , $i = x, y, z$, are acting in the valley, sublattice and spin space, respectively, while we set $\hbar v_F \equiv 1$.

A domain wall (DW) in one of the couplings $\Delta \in \{m, \lambda_{KM}, \lambda_{VZ}, \lambda_R\}$ (the other couplings are kept constant, possibly zero) is defined as:

$$\Delta(x) \equiv \frac{\Delta_L + \Delta_R}{2} + \frac{\Delta_R - \Delta_L}{2} \eta(x), \quad (2)$$

characterized by the limiting values $\Delta_L \equiv \Delta(x \rightarrow -\infty)$, $\Delta_R \equiv \Delta(x \rightarrow \infty)$, which define the domains to the left and to the right of the DW, and by an arbitrary smooth function $\eta(x)$, which satisfies $\eta(x \rightarrow \pm\infty) = \pm 1$ (see Fig. 1a). Focusing on a single DW, the DW profile $\eta(x)$ may be taken as monotonous, and its particular form has no bearing on the results in this section: one may imagine a typical profile such as $\eta(x) \in \{\frac{2}{\pi} \arctan(x/l), \tanh(x/l) \dots\}$ with a finite width lengthscale l . We only consider cases where both domains L, R have a full gap far away from the DW.

A. Spectral flow theorem: Kane-Mele spin-orbit and mass domain walls

The spectral flow theorem is presented in mathematical detail in Refs. [34, 35], while here we demonstrate its practical use in 2D with one spatially dependent coupling by solving step-by-step the DW in Kane-Mele coupling $\Delta(x) \equiv \lambda_{KM}(x)$ in presence of a constant mass term m . This example unifies two physical situations (Fig. 1c) as discussed below. The theorem involves a few steps:

1. We replace the quantum Hamiltonian of Eq. (1), $H(x, -i\partial_x, k_y)$, with a matrix function $\tilde{H}(x, k_x, k_y) = k_x \tau_z \sigma_x + k_y \sigma_y + m \sigma_z + \Delta(x) \tau_z \sigma_z s_z$ of classical variables so that k_x now commutes with x and thereby with $\eta(x)$ and $\Delta(x) \equiv \lambda_{KM}(x)$.

DW homog.	Dirac mass	Kane-Mele SOC	Valley-Zeeman SOC	Rashba SOC
Dirac mass	2xVAL	1x$\mathcal{H}\mathcal{E}\mathcal{L}$ \dagger	\emptyset	\emptyset
Kane-Mele SOC	1x$\mathcal{H}\mathcal{E}\mathcal{L}$ \dagger	2x $\mathcal{H}\mathcal{E}\mathcal{L}$	\emptyset	\emptyset
Valley-Zeeman SOC	2xVAL \ddagger	2x $\mathcal{H}\mathcal{E}\mathcal{L}$ \ddagger	X	\emptyset
Rashba SOC	2xVAL \ddagger	\emptyset	2xVAL	X

Table I. Propagating in-gap modes hosted on domain wall (DW) where one coupling (columns) changes sign, in presence of another homogeneous coupling (rows), or in absence of other couplings (on the diagonal). DWs considered here for the first time are shaded pink, while in red are new modes robust to intervalley lattice effects (italic), spin- S_z breaking (bold), and any value of Rashba SOC. We ignore combinations without bulk-gaps far away from the DW (X). Prefactors mark the number of helical pairs (HEL), or valley-polarized pairs (VAL). The Quantum Spin Hall edge modes (\dagger) appear if the homogeneous coupling dominates in one domain; if it does not dominate in either one reverts to modes on diagonal in the column. The modes \ddagger are continuation of modes on diagonal in the column, but being robust only up to a critical value the homogeneous coupling.

2. We consider \tilde{H} which have some gap in the spectrum that may close at most at some isolated points (x^i, k_x^i, k_y^i) labeled by an integer i . Physically, this requires that on both domains far away from the DW the H has a gap between, say the bands n and $n+1$, and we consider the lower n bands filled. The spectrum of our \tilde{H} is $E_{\tau s \pm} = \pm \sqrt{k_x^2 + k_y^2 + (\tau s \Delta(x) + m)^2}$, with $\tau = \pm$, $s = \pm$ being the eigenvalues of τ_z , s_z , respectively. We are interested in the gap opened at the Dirac point, i.e., half filling, so there are 4 filled bands $E_{\tau s -}$.
3. We identify at most two possible degeneracy points closing the gap between filled and empty bands, namely $(x^i, k_x^i, k_y^i) = (x_c^i, 0, 0)$ where $\tau s \Delta(x_c^i) + m = 0$ so that

$$\lambda_{KM}(x_c^i) = -\tau s m \in \{+m, -m\}, \quad (3)$$

and for our smooth monotonous DW profile $\eta(x)$ the equation over all τ, s has either:

- (a) No solutions for $|\Delta_L|, |\Delta_R| < |m|$ (both domains trivially gapped with the same mass),
- (b) One solution if $|\Delta_L| < |m| < |\Delta_R|$ or $|\Delta_L| > |m| > |\Delta_R|$ (edge between TI and trivial mass gap),
- (c) Both solutions for $|\Delta_L|, |\Delta_R| > |m|$ with $\text{sgn}(\Delta_L \Delta_R) < 0$ (DW between two TI domains of opposite sign of λ_{KM}).
4. We enclose a given degeneracy point (x^i, k_x^i, k_y^i) with a closed surface, e.g., sphere $S^i(\theta, \phi)$, and on this surface consider the projector \tilde{P}^i onto the filled bands of \tilde{H} (for a degeneracy line we need to adapt the enclosing surface, see Section II B 1). The spectral flow theorem states that the number of chiral modes N_{chiral}^i traversing the gap (more precisely, leaving the valence band) is:

$$N_{\text{chiral}}^i = C_{-}^i, \quad (4)$$

where the chiral modes of positive(negative) velocity along y are counted positively(negatively), and C_{-}^i is the first Chern number of the filled states on the sphere $S^i(\theta, \phi)$:

$$C_{-}^i = -\frac{1}{2\pi i} \int_0^{2\pi} d\phi \int_0^{\pi} d\theta \text{Tr} P_{-}^i (\partial_{\theta} P_{-}^i \partial_{\phi} P_{-}^i - \partial_{\phi} P_{-}^i \partial_{\theta} P_{-}^i). \quad (5)$$

The enclosing sphere $S^i(\theta, \phi)$ can be parametrized using $(x, k_x, k_y) = (x^i, k_x^i, k_y^i) + \epsilon(\delta x, \delta k_x, \delta k_y)$ with $(\delta x, \delta k_x, \delta k_y) \equiv (\cos(\theta), \sin(\theta) \cos(\phi), \sin(\theta) \sin(\phi))$, where it is only important to preserve the orientations of the coordinate systems, see Fig. 1b. The coupling term is also approximated on the sphere using the smoothness and monotonicity of the profile $\eta(x)$: $\tau s \Delta(x) + m \approx \tau s D_{RL} \delta x$, $D_{RL} \equiv \text{sgn}(\lambda_{KM,R} - \lambda_{KM,L})$ for the two possible degeneracy points, where we rescaled the coupling by a positive constant which does not change the topology of \tilde{P} (similarly we set the radius $\epsilon = 1$). The projectors to the 4 filled bands are

$$P_{\tau s, -}^i = \frac{1}{2} (\mathbb{1} - \hat{d}_{\tau s}^i \cdot \sigma) \quad (6)$$

$$\hat{d}_{\tau s}^i = (\tau \sin(\theta) \cos(\phi), \sin(\theta) \sin(\phi), \tau s D_{RL} \cos(\theta)). \quad (7)$$

The standard Chern number of spin-1/2 in magnetic field implies that $C_{\tau s, -} = s D_{RL}$, since C is preserved under inversion of \hat{d} but flips sign under mirror operations. A band contributes one mode ($|C_{\tau s, -}| = 1$) for each degeneracy point its τ, s give according to Eq. (3). In particular, if $\lambda_{KM,R} > \lambda_{KM,L}$ then a KM DW profile $\lambda_{KM}(x)$ which crosses the value m hosts two chiral modes (Kramers pair) with quantum numbers $\tau = -s$, while if it crosses the value $-m$ there are two (more) modes with $\tau = s$, with chiralities always $N_{\text{chiral}} = s$.

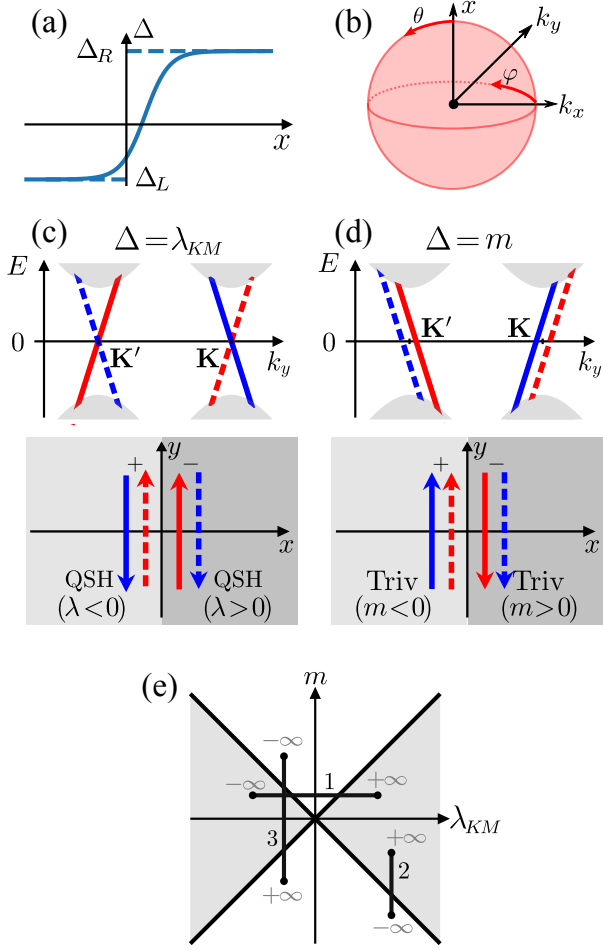


Figure 1. Spectral flow theorem for domain walls (DW) in Kane-Mele (KM) spin-orbit coupling λ_{KM} and mass m in the continuum. (a) Generic profile of a continuum DW with arbitrary asymptotic values Δ_L, Δ_R on the two domains. (b) A degeneracy point in classical variable space is enclosed by a sphere $S^2(\theta, \phi)$ on which one calculates the Chern number of the projector to states below the gap. (c) Sketch of modes predicted by the theorem for a KM DW at arbitrary constant mass, in momentum space (top; note that the K and K' are actually located at the same continuum momentum $k_y = 0$, offset for visibility) and in real space (bottom). Red(blue) is spin S_z up(down), arrow denotes mode's group velocity, while \pm are two valleys. When $\lambda_{KM}(x)$ passes through value m the full-line modes appear, and when it passes $-m$ the dashed ones do. Edge of a QSH state corresponds to $|m|$ dominating in one of the domains, so only one Kramers pair of modes appears. (d) As in (c) but for a DW in mass coupling at constant λ_{KM} . (e) A DW phase diagram for arbitrary smooth DW profile: points $\pm\infty$ are values of $(\lambda_{KM}(x), m(x))$ at $x \rightarrow \pm\infty$. The DW may create any path, and a Kramers pair of modes appears for every time a diagonal boundary line is crossed (the valley number of modes is opposite for two diagonals). Three paths (chosen straight) exemplify cases in (c,d): sign-changing KM DW (line 1; all 4 modes in (c)), QSH edge (line 2; two modes in (c)), and mass DW (line 3; in (d)).

The obtained modes of a KM DW are sketched in Fig. 1c. As expected we recover the Kramers pair of TI edge modes. For the case of a DW at which λ_{KM} changes sign (while $|m| < |\lambda_{KM,R}|, |\lambda_{KM,L}|$, possibly $m = 0$), the Z_2 Fu-Kane invariant of a TI predicts no modes protected by time reversal symmetry. The two Kramers pairs predicted above for this DW are rather associated with each domain's spin-Chern number[29, 30], whose sign follows the sign of λ_{KM} . Therefore these modes should be protected by spin S_z conservation, which we confirm in the next Section.

Using the above approach we also find the well-known valley-polarized modes for a DW with a sign change of mass m (given that $|\lambda_{KM}| < |m_R|, |m_L|$), Fig. 1d.[15, 34] The total phase diagram of DWs in KM and mass is shown in Fig. 1e. In contrast to these cases, a DW in either λ_{VZ} or λ_R in presence of a constant m does not host any gapless modes. Concretely, in the first case the spectrum of \tilde{H} is $E_{\tau s} = \tau s \lambda_{VZ} \pm \sqrt{k^2 + m^2}$, which is either gapless or has no degeneracy point, while in the second case $E_{\alpha\beta} = \alpha \sqrt{k^2 + m^2 + 2\lambda_R^2} + 2\beta |\lambda_R| \sqrt{k^2 + \lambda_R^2}$, with $\alpha, \beta = \pm$, has no degeneracy points for any value of $\lambda_R(x)$. A DW in presence of λ_{VZ} and λ_R presents new modes, and is discussed in the next subsection II B.

How much protection is guaranteed for these DW modes by the spectral flow theorem? The theorem is topological so each chiral mode is *a priori* protected against smooth deformations of the profile $\eta(x)$ and all other perturbations which do not close the gap of \tilde{H} outside a small sphere enclosing the degeneracy point. The theorem also provides the exact chiralities of the modes labeled by quantum numbers, and since in the above cases the Hamiltonian reduces to a 2x2 matrix we are able to confirm these predictions by constructing the exact wavefunctions of the modes of a DW with arbitrary profile (Appendix A). In any case our modes are labeled by valley and spin numbers τ, s , so even the topological theorem cannot prevent mixing of modes inside the bulkgap in case these numbers become ill-defined, which is investigated in Section III.

B. Valley-Zeeman and Rashba spin-orbit couplings

We use the spectral flow theorem to show that a DW in VZ spin-orbit coupling in presence of Rashba spin-orbit hosts propagating modes which were not identified before. Conversely, a DW in Rashba has no gapless modes.

First of all, a domain with constant $\lambda_{VZ}, \lambda_R \neq 0$ has a gap $\frac{2|\lambda_R \lambda_{VZ}|}{\sqrt{\lambda_R^2 + \lambda_{VZ}^2}}$ at half filling even though neither coupling on its own opens a gap in graphene. Let us therefore consider a DW: the auxiliary Hamiltonian \tilde{H} has the spectrum

$$E_{\tau, \alpha\beta} = \alpha \sqrt{k^2 + \lambda_{VZ}^2 + 2\lambda_R^2 + 2\beta \sqrt{\lambda_R^4 + (\lambda_R^2 + \lambda_{VZ}^2)k^2}}, \quad (8)$$

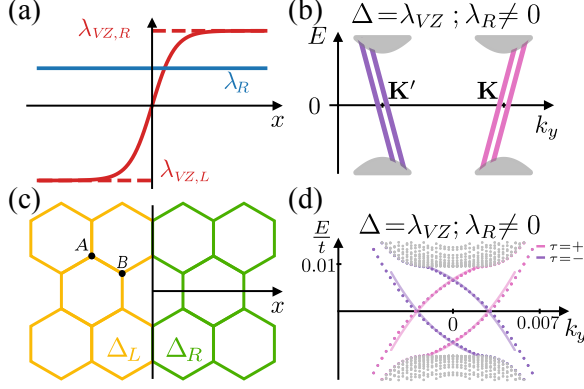


Figure 2. Valley-Zeeman (VZ) DW modes and their robustness on the lattice. (a) Generic profile of sign-changing VZ DW, with arbitrary value of Rashba SOC λ_R . (b) Sketch of modes in momentum space predicted by spectral flow theorem for a VZ DW in (a). (c) Definition of lattice with left and right domains for an atomically sharp profile of an armchair DW. (d) Tight-binding lattice model spectrum for an armchair VZ DW such as in (c), with parameters $N_x = 801$, $N_y = 2000$, $\lambda_{VZ}(\pm\infty) = \pm 0.01t$ and $\lambda_R = 0.1t$. The in-gap modes match continuum theory in (b), with purple/pink being states in valley K/K' (both valleys project to $k_y = 0$ on the lattice), and match the spectrum of DW in gating of bilayer graphene (full lines; see text).

with $\alpha, \beta = \pm$, and a valley degeneracy of each band. As noted, this spectrum has a gap if $\lambda_{VZ}, \lambda_R \neq 0$. We are interested in a degeneracy at half filling, i.e., between the two inner bands, the $\alpha = \pm$ and $\beta = -$. Consequently, for a given τ we construct the 4×4 projector to the 2 filled bands of \tilde{H} on the parametrized surface enclosing the degeneracy: $P_\tau = P_\tau^{\alpha=-, \beta=+} + P_\tau^{\alpha=-, \beta=-}$, using the formula for the projector to the n -th band: $P^{(n)} = \prod_{m \neq n} \frac{\tilde{H} - E_m}{E_n - E_m}$. Now we are ready to study two types of DWs, either in λ_R or in λ_{VZ} , and find new topological modes on the latter one.

1. Rashba domain wall and constant Valley-Zeeman

First we consider a DW in $\Delta(x) \equiv \lambda_R(x)$ constant $\lambda_{VZ} \neq 0$ which implies that a degeneracy at half-filling occurs on a ring

$$(x^\phi, k_x^\phi, k_y^\phi) = (x_c, |\lambda_{VZ}| \cos(\phi), |\lambda_{VZ}| \sin(\phi)), \quad (9)$$

where $\lambda_R(x_c) = 0$. Therefore propagating modes are *a priori* possible only if the Rashba coupling changes sign across the DW. The spectral flow theorem dictates that we enclose the entire line of degeneracy points with a surface, in this case the ring is simply enclosed by a torus of small radius ϵ :

$$\begin{pmatrix} \lambda_R \\ k_x \\ k_y \end{pmatrix} = \begin{pmatrix} \epsilon \cos(\theta) \\ (|\lambda_{VZ}| + \epsilon \sin(\theta)) \cos(\phi) \\ (|\lambda_{VZ}| + \epsilon \sin(\theta)) \sin(\phi) \end{pmatrix} \quad (10)$$

The Chern number of the projector onto the filled bands over the torus surface (one just changes the range of $\theta \in [0, 2\pi]$ in Eq. (5)) gives zero, and therefore there are no topological gapless modes on the Rashba DW.

2. New topological modes: Valley-Zeeman domain wall and constant Rashba

Here we look for gap-closing points with a changing $\Delta(x) \equiv \lambda_{VZ}(x)$ at a constant $\lambda_R \neq 0$: the gap closes at most at one point $(x, k_x, k_y) = (x_c, 0, 0)$ if $\lambda_{VZ}(x_c) = 0$ occurs.

The calculation for projectors as in Section II B 1 but parametrized on a sphere S^2 results in Chern numbers $C_\tau = 2\tau \operatorname{sgn}(\lambda_{VZ,R} - \lambda_{VZ,L})$.

The outcome of the spectral flow theorem is that a DW across which λ_{VZ} changes sign, in presence of any non-zero λ_R (Fig. 2a), has two valley-locked propagating modes (Fig. 2b). In this way the modes resemble the ones on a DW in m , however they don't have a spin quantum number attached, and will turn out to be much more robust (Section III).

It is very important to clarify that these VZ DW modes are not at all the same as the zigzag ribbon edge modes of graphene with λ_{VZ} in the so-called "quantum valley spin Hall state" (QVSHS) demonstrated in Ref. [22]. First, we have two co-propagating modes per DW in each valley due to $|C_\tau| = 2$, while the QVSHS has one mode per edge in each valley associated to a valley-Chern number $|C_v| = 1$. (Note, the additional "pseudohelical modes" of QVSHS connect valleys, so they cannot be matched to our DW modes). Second, the QVSHS modes are destroyed by increasing λ_R/λ_{VZ} , while for our VZ DW the topology is completely independent of the value $\lambda_R \neq 0$. Third, and most strikingly, the QVSHS valley edge modes are very fragile, in particular they are completely gapped on an armchair edge where the two valleys are projected onto each other; in contrast we will show that our VZ DW modes are robust to intervalley scattering even in the armchair direction and an atomically sharp DW profile (Section III).

The VZ DW modes can actually be exactly mapped onto the bound states of a gate voltage DW in spinless bilayer graphene introduced in Ref [11]. The low energy Hamiltonian of AB-stacked gated bilayer graphene (BLG) is:

$$H_{BLG} = k_x \sigma_x + k_y \tau_z \sigma_y + \frac{t_\perp}{2} (\sigma_x \eta_x + \sigma_y \eta_y) - V \eta_z, \quad (11)$$

where the new Pauli matrices η_i act in the layer space, while t_\perp is the hopping amplitude to go from the A atom of one layer to a B atom of the other layer. The mapping to our VZ+R model can be done stepwise by applying two unitary transformations. First, to recover our form of the kinetic part we apply $U^\dagger = \frac{1+\tau_z}{2} + \frac{1-\tau_z}{2} \sigma_z$ which

multiples the $\tau = -1$ sector by σ_z , obtaining

$$H_{BLG}^{(1)} = k_x \tau_z \sigma_x + k_y \sigma_y + \frac{t_\perp}{2} \tau_z (\sigma_x \eta_x + \sigma_y \eta_y) - V \eta_z \quad (12)$$

Second, we map the layer exchange part onto Rashba SOC and the gate voltage to VZ SOC by performing a rotation around η_z to exchange x and y , and then multiplying by η_y in the $\tau = -1$ sector, which altogether requires $U^\dagger = \frac{1-i\eta_z}{\sqrt{2}} (\frac{1+\tau_z}{2} + \frac{1-\tau_z}{2} \eta_y)$, so that in the end we have

$$H_{BLG}^{(2)} = k_x \tau_z \sigma_x + k_y \sigma_y + \frac{t_\perp}{2} (\tau_z \sigma_x \eta_y - \sigma_y \eta_x) - V \tau_z \eta_z. \quad (13)$$

By reinterpreting the spinless BLG's layer degree of freedom as a spin degree of freedom we finally get the Hamiltonian of graphene with a VZ SOC $\lambda_{VZ} = -V$ and a Rashba SOC $\lambda_R = \frac{t_\perp}{2}$.

In the limit where $V \ll t_\perp \Rightarrow \lambda_{VZ} \ll \lambda_R$ which was studied in Ref. [11] they show that for $V(x) = \kappa V_0 \text{sgn}(x)$ with $t_\perp > 0$, $V_0 > 0$, and $\kappa = \pm 1$, there are 4 in-gap branches crossing zero energy:

$$E_{\tau\pm} = \pm \left(\frac{v_F k_y \tau \kappa}{2\sqrt{t_\perp}} \mp \sqrt{\frac{v_F^2 k_y^2}{4t_\perp} + \frac{V_0}{\sqrt{2}}} \right)^2 \mp \sqrt{2} V_0. \quad (14)$$

The crossings appear at $k_y = \mp \frac{\kappa}{v_F} \sqrt{\frac{t_\perp V_0}{2\sqrt{2}}}$, while the sign of the velocity around the crossings is given by $-\kappa \tau$. Given the identification $\lambda_{VZ}(x) = -V(x)$, it means that for a DW with negative values of VZ on the left and positive values on the right, the bound states with $\tau = 1$ are right movers, which matches our tight-binding calculations, Fig. 2d (k_y units for continuum and lattice are matched using free graphene).

III. ROBUSTNESS: DOMAIN WALLS ON THE LATTICE

In the continuum theory the in-gap modes hosted by DWs are labeled by at least a valley index τ , and possibly also a spin S_z quantum number s , so even the topological theorem cannot prevent the mixing of modes in case these numbers become ill-defined. Therefore in this Section we study via exact diagonalization the tight-binding lattice models of these DWs with three main goals: (i) To confirm the continuum theory predictions when DW profile varies slowly over many lattice sites; (ii) To assess the robustness to intervalley scattering and lattice anisotropy using an atomically sharp DW profile, and (iii) To assess the robustness to including all spin-orbit terms simultaneously, which as benefit removes any spin-rotation symmetry of the continuum modeling.

The tight-binding Hamiltonian collecting all the

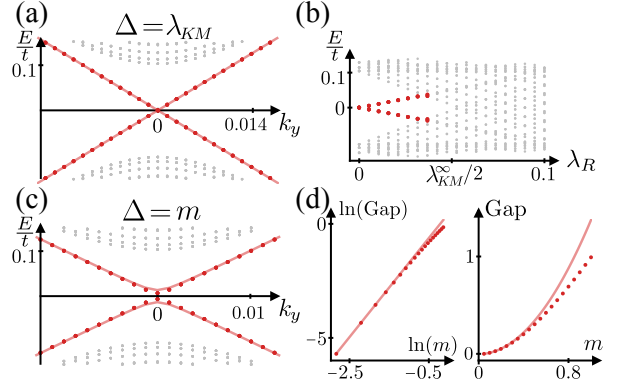


Figure 3. Robustness of KM and mass sharp DWs on the lattice (see Fig. 2c). (a) Tight-binding lattice model spectrum for a sign-changing KM DW, with parameters $N_x = 204$, $N_y = 500$, $\lambda_{KM}(\pm\infty) = \pm 0.1t$. The in-gap modes match continuum theory in Fig. 1c and are robust to intervalley scattering. (b) The spectrum of DW in (a) at momentum $k_y = 0$, showing a gap in DW modes with increasing Rashba coupling λ_R . (c) Tight-binding lattice model spectrum for a sign-changing mass DW, with parameters $N_x = 204$, $N_y = 500$, $m(\pm\infty) = \pm 0.1t$. The DW modes predicted in Fig. 1d are gapped due to intervalley scattering. (d) The gap size in at $k_y = 0$ in mass DW modes from (c), measured in tight-binding (dots) and derived perturbatively (line; Appendix B), as function of $m \equiv |m(x \rightarrow \pm\infty)|$ (energy unit is t).

position-dependent coupling terms we consider is:

$$H = -t \sum_{\langle i,j \rangle} c_i^\dagger c_j + \sum_{i,\alpha} (-1)^{l_i} m_i c_{i\alpha}^\dagger c_{i\alpha} \quad (15) \\ + i \sum_{\langle\langle i,j \rangle\rangle, \alpha, \beta} \lambda_{ij}^{KM} \nu_{ij} c_{i\alpha}^\dagger s_z^{\alpha\beta} c_{j\beta} + H.c. \\ + i \sum_{\langle\langle i,j \rangle\rangle, \alpha, \beta} \lambda_{ij}^{VZ} (-1)^{l_i} \nu_{ij} c_{i\alpha}^\dagger s_z^{\alpha\beta} c_{j\beta} + H.c. \\ + i \sum_{\langle i,j \rangle, \alpha, \beta} \lambda_{ij}^R \hat{z} \cdot (\vec{d}_{ij} \times \vec{s}^{\alpha\beta}) c_{i\alpha}^\dagger c_{j\beta} + H.c.,$$

where $c_{i\alpha}^\dagger$ creates an electron on site i with S_z spin $\alpha = \pm$, the $(-1)^{l_i} = +(-)$ for a site on sublattice $A(B)$, the $\nu_{ij} = \text{sgn}[\hat{z} \cdot (\vec{d}_{ij}^{(1)} \times \vec{d}_{ij}^{(2)})]$ with $\vec{d}_{ij}^{(1)}, \vec{d}_{ij}^{(2)}$ the two NN-bond vectors forming the path $j \rightarrow 1 \rightarrow 2 \rightarrow i$ between NNN neighbors j, i , where we normalize $|\vec{d}_{ij}| = 1$. When the couplings are constant, independent of sites i, j , one finds the quantitative connection to the continuum couplings, i.e., $m_i = m$, $\lambda_{KM} = -3\sqrt{3}\lambda_{ij}^{KM}$, $\lambda_{VZ} = -3\sqrt{3}\lambda_{ij}^{VZ}$, $\lambda_R = -3\lambda_{ij}^R/2$.

Now we consider a DW profile $\eta_i(\vec{R}_0) = \tanh \left[\frac{(\vec{R}_i - \vec{R}_0) \cdot \vec{e}_{DW}}{l} \right]$, where \vec{R}_i is the position of site i , \vec{R}_0 is a position in the center of a honeycomb plaquette, while the $\vec{e}_{DW} = \hat{x}(\hat{y})$ gives an armchair(zigzag) DW on the lattice, Fig. 2c. We consider periodic boundary conditions and therefore

a DW—anti-DW pair at maximum separation in the finite system, $\eta_i = \eta_i(\vec{R}_{DW}) - \eta_i(\vec{R}_{antiDW})$. One of the couplings has a DW profile according to $\Delta_i \equiv \Delta\eta_i$ for $\Delta_i \in \{m_i, \lambda_{ij}^{KM}, \lambda_{ij}^{VZ}, \lambda_{ij}^R\}$, while the rest are constant (possibly zero). Note, since the bulkgap is given by the smaller of the bulkgaps on two domains, for simplicity our profile has $\Delta_L = \Delta_R \equiv \Delta$. The Hamiltonian has translational symmetry along the straight DW, and consequently the bulk Dirac points are projected onto two distant momenta k_x in case of zigzag DW, and onto the same $k_y = 0$ in case of armchair DW. Effects of intervalley scattering are consequently masked in the zigzag DW case, and we find the predicted continuum modes. Therefore in the rest of the paper we present the armchair DWs for which the intervalley lattice scattering effects are fully exhibited. The length l is used to vary the smoothness of the DW profile and therefore tune the amount of intervalley scattering. By “sharp DW” we mean the limit $l \rightarrow 0$, where $\eta_i(\vec{R}_0)$ becomes a step-function (Fig. 2c). For a sharp DW we verify that the precise value of couplings on NNN bonds which cross the domain boundary do not matter for the main features of in-gap modes. To distinguish the DW and anti-DW in-gap states, we energetically split them by adding a small localized chemical potential at the DW. To assign a valley index to an in-gap state, we use a Fourier transform of x , for which the valleys occur at different momenta.

Starting with a DW in Valley-Zeeman and a constant Rashba coupling, we find two copropagating modes in each valley per DW in exact accord with the new modes identified in the continuum in Section II B 2; the modes in tight-binding persist even for a sharp DW profile, Fig. 2d, compare to continuum result in Fig. 2b. To further test the robustness of these DW modes, we add a constant λ_{KM} coupling, which is a natural choice since all three types of spin-orbit appear in graphene on TMD substrate[2, 3, 8–10]. The in-gap modes indeed stay gapless with increasing λ_{KM} all the way until the bulkgap opened by λ_{VZ} and λ_R closes, which happens when it is surpassed in value by λ_{KM} . The competing bulkgaps were already identified in Refs. [22, 23].

In contrast, a domain wall in the Rashba coupling with a constant Valley-Zeeman shows no gapless modes on the lattice, even for smooth DW profiles, as expected from the trivial topology in the continuum, Section II B 1.

Switching to Kane-Mele coupling, on the lattice the DW by our definition exhibits a change in sign of λ_{KM} , so for simplicity we take m (and other couplings) to zero. As expected from the continuum (Fig. 1c), we find (Fig. 3a) two copies of Quantum Spin Hall helical modes per DW. As argued already, these modes are not anymore protected by time reversal (Z_2 index), and *a priori* should be fragile. Somewhat surprisingly we find that they are robust to intervalley scattering and persist even for a sharp DW. In contrast, any non-zero constant λ_R term gaps out the helical modes by an amount proportional to λ_R (Fig. 3b), thereby confirming that their protection is

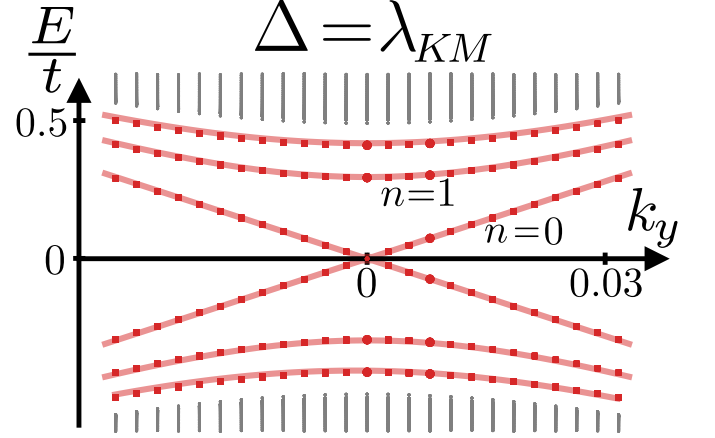


Figure 4. Excited states of a smooth sign-changing KM DW, $\lambda_{KM}(+\infty) \equiv -\lambda_{KM}(-\infty)$, compared on lattice and in continuum. Tight-binding model (red dots) has $|\lambda_{KM}(+\infty)| = 0.5t$, and the width of the domain wall is $l = 20$ sites. Analytical solution of continuum theory (red lines) matches the form of Landau levels of spinless graphene with effective magnetic field $B_{eff} \propto \frac{1}{v_F} \frac{d\lambda_{KM}}{dx}|_{x_0}$ given by slope of DW profile at $\lambda_{KM}(x_0) = 0$.

due to spin S_z conservation.

Finally we consider the well-known modes of a sign-changing DW in the mass m . They are fragile to intervalley scattering (Fig. 3c),[15] but here we are able to quantify the effect. Treating a sharp DW as a perturbation to ideal graphene (Appendix B), we find that intervalley scattering at second order opens a gap of size $2\frac{2m^2}{3t}$ in the DW modes, which matches very well the tight-binding results, Fig. 3d. Our perturbative approach is applicable only if $m < t$, which translates to the gapped DW modes still remaining inside the bulkgap. Interestingly, even a small smoothing of the DW profile, e.g., to a width of few lattice constants $l \sim 2a$, drastically reduces, e.g., by an order of magnitude, the intervalley effect at second order and the gap in the modes (see Appendix B).

IV. EXCITED MODES ON A KANE-MELE DOMAIN WALL: LANDAU LEVELS

We found that a sign-changing DW of λ_{KM} hosts two pairs of helical modes which are robust to intervalley scattering but sensitive to breaking spin S_z conservation (Sections II A, III). In a system such as graphene on TMD substrate, magnetic impurities are rare and the spin symmetry breaking would likely come from the Rashba term, which is however experimentally found to be much weaker than the induced Kane-Mele and Valley-Zeeman terms[2, 3]. Additionally, even gapped modes bound to a linear defect are useful to probe the state of the system. Therefore we reconsider the Kane-Mele DW from the aspect of excited modes. Inspired by Ref. [38] we start with a very smooth DW profile in the continuum,

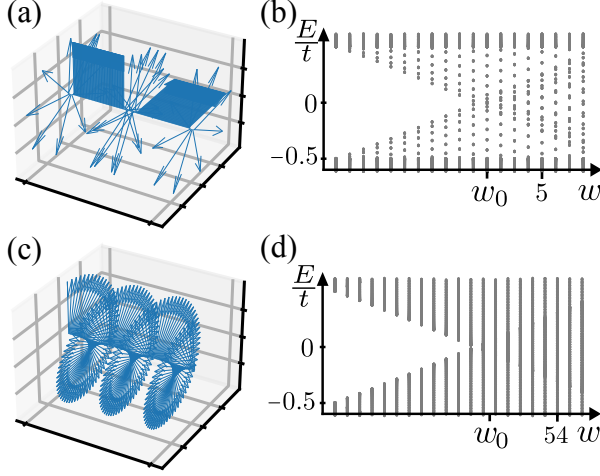


Figure 5. Spiraling DW in KM coupling. (a) Arrows show the rotation of spin-axis in KM SOC (see text), there are two domains in a periodic system with length $N_x = 204$ sites. The DW width ξ is 20 sites. (b) Low energy states at $k_y = 0$ for a spiralling Kane-Mele spin-orbit of amplitude $|\vec{\lambda}| = 0.5t$. The prediction for gap-closing value is w_0 (see text). (c,d) As (a,b) but for a bulk spiral.

so that in a large region of space it is a good approximation to linearize the profile $\eta(x)$. Doing so gives a Hamiltonian which is very similar to the Hamiltonian of Landau levels in graphene. Concretely, we obtain two series of two-fold degenerate states:

$$E_n(q_y) = \pm \sqrt{2v_F \frac{\lambda_0}{l} n + v_F^2 q_y^2}, \sqrt{2v_F \frac{\lambda_0}{l} (n+1) + v_F^2 q_y^2} \quad (16)$$

where $n = 0, 1, 2, \dots$, the DW slope is $\frac{\lambda_0}{l} \equiv \frac{d\lambda_{KM}}{dx} \big|_{x_0}$, with x_0 being defined by $\lambda_{KM}(x_0) = 0$. For typical DW profiles the value $\lambda_0 = \lambda_{KM}(+\infty) - \lambda_{KM}(-\infty)$. In total, the level at $n = 0$ is two-fold degenerate, and all others are four-fold, which matches the Landau levels of spinless graphene in an effective magnetic field of $v_F \lambda_0 / l$. The predicted Landau-like levels match perfectly the tight-binding KM DW with a profile smooth on the nanoscale, i.e., having width $l = 20\sqrt{3}a$, Fig. 4. Clearly, the $n = 0$ modes are the gapless linear modes which persist when the domain wall width l goes to zero (if S_z is conserved), while the $n > 0$ modes leave the bulkgap. More precisely, the number of DW excited modes inside the bulkgap is estimated as $n_{max} \sim \frac{|\lambda_{KM}(\pm\infty)|}{t} \frac{l}{a}$.

V. SPIRALING DOMAIN WALL IN KANE-MELE SPIN-ORBIT COUPLING

From the perspective of unifying topological modes due to inhomogeneous spin-orbit coupling, one may note that a sign-changing DW in λ_{KM} can either host robust modes (on a QSH edge, e.g., $|\lambda_{KM,L}| < |m| <$

$|\lambda_{KM,R}|$), or modes sensitive to S_z breaking (e.g., when $|m| < |\lambda_{KM,L}|, |\lambda_{KM,R}|$), raising the question whether there are DWs in λ_{KM} which break S_z by design but whose modes are not equivalent to QSH edge modes. A natural candidate is a DW across which the spin-axis of Kane-Mele coupling rotates. From a different viewpoint, the idea that a spiralling magnetic coupling emulates a constant spin-orbit coupling[39] has been fruitful in designing topological modes, so it is natural to ask what modes are associated with a spiralling spin-orbit coupling.

The tight-binding lattice model of a spiralling Kane-Mele DW, Fig. 5a, consists of two domains with a well defined spin-axis of KM SOC, i.e. $H_{KM,rot}(x \rightarrow \pm\infty) = \lambda \tau_z \sigma_z \hat{e}_z \cdot \hat{R}(\theta_{R/L}) \vec{s}$, where $\hat{R}(\theta)$ is a rotation matrix acting on spin vector. The DW between domains has width ξ across which spin axis rotates linearly in x . In particular we rotate the original s_z around the x -axis:

$$\mathcal{H}_{spir,L/R} = \lambda \tau_z \sigma_z \begin{pmatrix} 0 \\ \sin(\theta_{L/R}) \\ \cos(\theta_{L/R}) \end{pmatrix} \cdot \vec{s} = \lambda \exp(i\theta_{L/R} s_x) \tau_z \sigma_z s_z \quad (17)$$

$$\begin{aligned} \mathcal{H}_{spir,DW} &= \lambda \tau_z \sigma_z \begin{pmatrix} 0 \\ \sin(2\pi w x / \xi + \theta_L) \\ \cos(2\pi w x / \xi + \theta_L) \end{pmatrix} \cdot \vec{s} \\ &= \lambda \exp((2i\pi w x / \xi + \theta_L) s_x) \tau_z \sigma_z s_z, \end{aligned} \quad (18)$$

where $\mathcal{H}_{spir,L}$ is used for $x < 0$, $\mathcal{H}_{spir,R}$ is used for $x > \xi$, and $\mathcal{H}_{spir,DW}$ is used for $0 < x < \xi$. The winding number w of the domain wall counts the number of revolutions of the spin axis around spin x -axis across the DW and is such that $2\pi w \equiv \theta_R - \theta_L \bmod 2\pi$. We can always perform a global rotation around s_x to send θ_L to 0. In Fig. 5a each arrow shows the local direction of the spin axis $\hat{R}(\theta(x)) \vec{s}$ as a function of the x coordinate. We use periodic boundary conditions so that there is an anti-DW with opposite winding located at the edge of the system.

As shown in Fig. 5b we do not find in-gap modes, but instead a bulkgap which linearly closes with the momentum of the spiral. Since we find that the evolution of the spectrum depends only on the parameters of the DW and not on those of the domains, we are probably observing a simple scattering effect. So we now focus on the spiralling term by considering a Hamiltonian with a spiral throughout the bulk, Fig. 5c:

$$\mathcal{H}_{KM,bulk} = \lambda \tau_z \sigma_z \begin{pmatrix} 0 \\ \sin(k_0 x) \\ \cos(k_0 x) \end{pmatrix} \cdot \vec{s} = \lambda \exp(ik_0 x s_x) \tau_z \sigma_z s_z. \quad (19)$$

We undo the spiral rotation with the following unitary transformation: $U = \exp(-i\frac{k_0}{2} x s_x)$. $\mathcal{H}_{KM,bulk}$ is sent to a constant Kane-Mele spin-orbit of amplitude λ . The ideal graphene kinetic term simply shifts by an SU(2)

gauge potential directed along x :

$$U\mathcal{H}_{tot,bulk}U^\dagger = -v_F \left(\tau_z \sigma_x \left(q_x + s_x \frac{k_0}{2} \right) + \sigma_y q_y \right) + \lambda \tau_z \sigma_z s_z. \quad (20)$$

We see that the spiralling KM effectively induces a constant spin-dependent magnetic potential. Since there is still a chiral symmetry ($\sigma_z s_x$), we can easily obtain the spectrum by squaring the Hamiltonian.

$$\text{Sp}(\mathcal{H}_{tot,bulk}^2) = \left\{ \left(v_F \frac{k_0}{2} \pm \sqrt{\lambda^2 + v_F^2 q_x^2} \right)^2 + v_F^2 q_y^2 \right\}. \quad (21)$$

The bulkgap is reduced as the valence and conduction bands move in opposite directions linearly with the spiral momentum k_0 . There are then two phases depending on k_0 . If $|k_0| < \frac{2|\lambda|}{v_F}$, the system is gapped at $(q_x, q_y) = (0, 0)$ and the gap is $2|\lambda| - v_F|k_0|$. Else, the system is gapless. Hence, we recovered the linearly closing gap and we predict a gap closing at $k_0 = \frac{2|\lambda|}{v_F}$. For the system in Fig. 5c, $k_0 = \frac{2\pi w}{\sqrt{3}N_x a}$ where w is the winding number. Consequently, we predict that the gap closing should occur at $w_0 = \frac{\sqrt{3}N_x a |\lambda|}{\pi v_F}$, that with $|\lambda| = 0.5t$ gives $w_0 = \frac{N_x}{\sqrt{3}\pi} \sim 37.5$. The tight-binding result in Fig. 5d has a gap closing at $w_0^{TB} = 34$. For the bulk spiral in Fig. 5b we reiterate this formula using $N_x = \xi$ and obtain $w_0 \sim 3.7$, while the tight-binding result is $w_0^{TB} = 3.4$. Therefore the simple bulk modes of a bulk spiral explain well the modes found on a spiral confined within the width of a DW.

VI. DISCUSSION AND CONCLUSIONS

Using the spectral flow theorem we derived topologically protected electronic modes of various domain walls in graphene with mass, Kane-Mele, Valley-Zeeman and Rashba SOC, with precise symmetry and chirality labeling. However this method does not address the robustness to breaking symmetries and to lattice effects, for which we employed tight-binding modeling.

One main finding is the robust pair of Kramers pairs on a VZ DW in presence of Rashba SOC, which might be relevant to the efforts of inducing topological phases in graphene by proximity to TMDs. Namely, the VZ SOC seems to be strongly present, with a weaker Rashba, at least on a large-scale average.[2, 3] Due to incommensurability, on at least the Moire pattern scale there can be domains where couplings vary significantly and even change sign. The Rashba coupling could possibly be made constant on larger domains by external fields. Altogether the VZ DW states may form a tunable network of propagating states between domains[4, 6, 18, 19, 36, 40]. For untwisted graphene on TMDs the Moire pattern is on the nanoscale, which might allow the propagating states to

remain well-defined, but also might lead to collective effects due to their real-space overlap. Spectroscopic measurements on the nanoscale might be useful to look for the modes, while it would be interesting to expand this study with the effects of local strain due to incommensurability.

The connection between VZ DW and a DW in gating of spinless BLG implies possibilities to explore valleytronics ideas. Since the VZ DW modes are not doubled compared to spinful BLG, and since they lack any spin-rotation symmetry, they should be more resilient to time-reversal breaking. The spinful gated BLG setup was used in Ref. [37] to engineer helical modes by magnetic field, and it is an interesting question how the VZ DW modes could be manipulated using external fields.

Another main finding is that a sign-changing DW of KM, topologically (in terms of Z_2 Fu-Kane invariant) equivalent to putting two QSH domains next to each other, hosts modes robust to lattice scattering but sensitive to breaking the spin-axis rotation symmetry. The TMD-induced Rashba coupling in graphene seems smaller than the total of VZ and KM couplings by an order of magnitude, so it is possible that the gap in KM DW modes is small and in-gap modes are present. Additionally, the gapped excited DW modes would also be inside the bulkgap if the KM DW is smooth enough, e.g., for $|\lambda_{KM}| \sim 10\text{meV}$ having width 70nm, which might be relevant for twisted incommensurate situations with large Moire periods.

More generally, our work should motivate further theoretical study of topological defects in spin-orbit coupling, as a domain wall is just the simplest one-dimensional example while zero-dimensional defects in spin-orbit coupling were confirmed to host interesting bound states[41, 42]. Methodically, the spectral flow theorem proved useful and informative in understanding one-dimensional defects in two spatial dimensions because the resulting three-dimensional parameter space had point- and line-like degeneracies in our models. It would be interesting to generalize this approach to defects in multiple parameters and in higher dimensions.

Appendix A: Exact solution of domain walls in Kane-Mele and mass couplings

In the continuum limit we are able to perform the calculation for a mass and SOC domain wall at the same time as opposed to the lattice calculation which will be performed later. Given the rotation invariance of the low-energy Hamiltonian we can consider a domain wall in the x direction without loss of generality. We start with Eq. (1) with the usual substitution $k_x \rightarrow -i\partial_x$:

$$\mathcal{H} = -iv_F \partial_x \tau_z \sigma_x + v_F k_y \sigma_y + \lambda(x) \tau_z s_z \sigma_z + m(x) \sigma_z. \quad (A1)$$

We rewrite the eigenproblem $\mathcal{H}\Psi = E\Psi$ as an explicit

first order differential equation :

$$\partial_x \Psi = \underbrace{\left(k_y \tau_z \sigma_z - \frac{\lambda(x)}{v_F} s_z \sigma_y - \frac{m(x)}{v_F} \tau_z \sigma_y + i \frac{E}{v_F} \tau_z \sigma_x \right)}_{\Lambda(x)} \Psi \quad (\text{A2})$$

Since Λ is block diagonal in the valley and spin space, we can compute the exponential in the different eigenspace independently. The general solution requires to compute the space ordered integral $\exp(\int_0^x \Lambda(t) dt)$. Since we are looking for zero modes, we restrict ourselves to $k_y = 0$ and $E = 0$ which makes the exponential easy to obtain. Doing so we will lose information on the chirality, but we will come back to it at the end. We introduce the following intermediate notations:

$$a(x) = \frac{1}{v_F} \int_0^x s^z \lambda(t) + \xi m(t) dt$$

so that $\int_0^x \Lambda(t) dt = -a(x) \sigma_y$ where ξ and s^z are respectively the eigenvalues of τ_z and s_z . As a consequence

$$\exp(-a(x) \sigma_y) = \text{ch}(a(x)) \mathbb{1} - \text{sh}(a(x)) \sigma_y. \quad (\text{A3})$$

Now we look for solutions of the differential equation which are normalizable. Let us assume that λ and m have finite limits in $\pm\infty$. Consequently

$$\begin{aligned} a(x) &\underset{+\infty}{\sim} \frac{1}{v_F} x (s^z \lambda_{+\infty} + \xi m_{+\infty}) = x a_+ \\ a(x) &\underset{-\infty}{\sim} \frac{1}{v_F} x (s^z \lambda_{-\infty} + \xi m_{-\infty}) = x a_- . \end{aligned}$$

This implies that

$$\exp(a \sigma_y) \underset{\pm\infty}{\sim} \frac{\exp(|a_{\pm} x|)}{2} \mathbb{1} - \text{sgn}(x a_{\pm}) \frac{\exp(|a_{\pm} x|)}{2} \hat{n} \cdot \vec{\sigma}. \quad (\text{A4})$$

To be normalizable, the divergent components of $\exp(a(x) \sigma_y)$ must be simultaneously zero at $\pm\infty$, which means that

$$\ker(\mathbb{1} - \text{sgn}(a_+) \sigma_y) \cap \ker(\mathbb{1} + \text{sgn}(a_-) \sigma_y) \neq \{0\}. \quad (\text{A5})$$

This is true if and only if $a_+ a_- < 0$.

If $m + \lambda$ changes sign, then we have a Kramers' pair with $\xi = s^z$. If $m - \lambda$ changes sign then we have an other one with $\xi = -s^z$.

Chirality can be most simply recovered in the limit of a wide DW, and we do not expect that chirality is flipped under smooth local deformations of the DW profile, including collapsing the DW into a discontinuous step-like potential. This limiting case can be fully solved with the previous method, albeit with more difficulties than for a smooth DW. Hence we will linearize the DW around a position where $\Delta = m + \xi s^z \lambda$ changes sign. We already

saw a change of sign in Δ is a sufficient and necessary condition for the zero modes.

$$\Delta = \frac{d\Delta(x)}{dx} \Big|_{x_0} (x - x_0) = \frac{\Delta_0}{l} (x - x_0), \quad (\text{A6})$$

where x_0 is the position where Δ goes to 0. Let's first focus on $k_y = 0$. By squaring the Hamiltonian we obtain an harmonic oscillator and an homogeneous term :

$$\mathcal{H}^2 = -v_F^2 \partial_x^2 + \frac{\Delta_0^2}{l^2} (x - x_0)^2 - v_F \frac{\xi \Delta_0}{l} \sigma_y. \quad (\text{A7})$$

The eigenenergies of the harmonic oscillator part are $2v_F |\Delta_0|/l (n + 1/2)$ with n a positive or null integer. The last term of Eq. A7 thus precisely shifts these energies to $2v_F |\Delta_0|/l n$ and $2v_F |\Delta_0|/l (n + 1)$. In particular the zero energy subspace is not degenerate as opposed to all other states which are two-fold degenerate and which contain both eigenvectors of σ_y . So, the zero energy eigenstate is also a eigenstate of σ_y with eigenvalue $\xi \text{sgn}(\Delta_0)$. And of course, if $m + \xi s^z \lambda$ changes sign, then $m + (-\xi)(-s^z) \lambda$ also changes sign in the same way.

Now, since $\mathcal{H}^2 = \mathcal{H}^2(k_y = 0) + v_F^2 k_y^2$, this means that the zero eigenvector of $\mathcal{H}(k_y = 0)$ has eigenvalue $\sigma_y v_F k_y$ where we identify σ_y with its eigenvalue. So, we recapitulate the chiralities of the different modes in the different cases in the following table :

		$m + \lambda$	$m - \lambda$
$\Delta_0 > 0$	$\Delta_0 < 0$	$\Delta_0 > 0$	$\Delta_0 < 0$
$+\uparrow \text{RM}$	$-\downarrow \text{RM}$	$+\downarrow \text{RM}$	$-\uparrow \text{RM}$
$-\downarrow \text{LM}$	$+\uparrow \text{LM}$	$-\uparrow \text{LM}$	$+\downarrow \text{LM}$

The first row denotes which term is changing sign while \pm is the value of ξ , \uparrow the value of s^z and RM (LM) means right (left) mover. The different transitions are summed up in the DW classification diagram Fig. 1e. So, for a DW between a trivial and QSH phase, then either $m + \lambda$ or $m - \lambda$ changes sign, but they cannot both change sign. We recover the standard edge states with direction of movement, spin and valley being correlated. If both terms change sign, then the DW separates either two trivial or two QSH phases. If it separate two trivial phases, then both $m + \lambda$ and $m - \lambda$ have the same sign. Thus, we have both spins at both valley, but valley and direction of movement are still correlated. If it separates two QSH phases, then $m + \lambda$ and $m - \lambda$ have opposite signs, so direction of movement is now only correlated with spin.

These match exactly the results of applying the spectral flow theorem.

Appendix B: Armchair domain wall in mass

Continuum theory predicts four in-gap states, with both spins present in both valleys. Here we consider an armchair domain wall in the mass term and perturbatively compute the valley-mixing effect near the Dirac

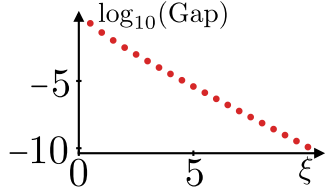


Figure 6. Exponential decay of the gap (in units of t) of the DW bound states as a function of the width of the domain wall (in units of lattice constant), for a mass DW.

$$H_{\text{trivial}} = \sum_{\beta=0}^{\frac{N_y}{2}-1} \sum_{\alpha=0}^{N_x-1} m_\alpha (c_{\alpha\beta, A1}^\dagger c_{\alpha\beta, A1} + c_{\alpha\beta, A2}^\dagger c_{\alpha\beta, A2} - c_{\alpha\beta, B1}^\dagger c_{\alpha\beta, B1} - c_{\alpha\beta, B2}^\dagger c_{\alpha\beta, B2}), \text{ where } m_\alpha = \begin{cases} +m & \text{if } \alpha < \frac{N_x}{2} \\ -m & \text{otherwise} \end{cases} \quad (B1)$$

Here we introduce an enlarged unit-cell comprising four atoms which belong to two adjacent elementary unit-cells. We use the numbers $\{1, 2\}$ to label this internal degree of freedom. This folds the hexagonal Brillouin zone

$$H_{\text{trivial}} = \sum_{k_y=0}^{\frac{N_y}{2}-1} \sum_{\substack{k_1=0 \\ k_2=0 \\ k_1-k_2 \equiv 1[2]}}^{N_x-1} m \frac{1}{N_x} \frac{4}{1 - e^{2i\pi \frac{(k_1-k_2)}{N_x}}} (c_{k_1 k_y, A1}^\dagger c_{k_2 k_y, A1} + c_{k_1 k_y, A2}^\dagger c_{k_2 k_y, A2} - c_{k_1 k_y, B1}^\dagger c_{k_2 k_y, B1} - c_{k_1 k_y, B2}^\dagger c_{k_2 k_y, B2}) \quad (B2)$$

Because we considered a sharp domain wall and symmetric domains we only couple states with an odd momentum difference. As a consequence there is no first order contribution of the mass on the Dirac cones, so we need to go to second order. To do so we need the eigenvectors with energies close to 0 which we obtain by using first order perturbation theory on the zero energy eigenspace of standard graphene but the perturbation is now the small momentum in the \vec{x} direction.

The Bloch Hamiltonian at the Dirac point $\mathbf{K} = \frac{N_x}{3} \vec{e}_x$ is, in units $t = -1$:

$$H_{\mathbf{K}} = \begin{pmatrix} 0 & 0 & 1 & -j^2 \\ 0 & 0 & -j & 1 \\ 1 & -j^2 & 0 & 0 \\ -j & 1 & 0 & 0 \end{pmatrix}, \quad (B3)$$

where $j = e^{\frac{2i\pi}{3}}$ is the usual cubic root of 1, and the Bloch Hamiltonian $H_{-\mathbf{K}}$ at the other valley $-\mathbf{K}$ is obtained simply by exchanging j and j^2 . Now we can compute the effect at first order, namely at first order in $\frac{p}{N_x}$,

momenta. Our initial eigenspace is the four-fold degenerate zero energy eigenspace for spinless fermions (so eight-fold for electrons) of standard graphene and our perturbation is the mass domain wall:

into a rectangle where $\pm\mathbf{K}$ are mapped to $\mp 2\pi/(3\sqrt{3}a)$.

The first step is to compute the matrix elements of the mass term in the Fourier basis.

$$H_{\mathbf{K}+p\vec{e}_x} = H_{\mathbf{K}} + \frac{2i\pi p}{N_x} \underbrace{\begin{pmatrix} 0 & 0 & 0 & j \\ 0 & 0 & -j^2 & 0 \\ 0 & j & 0 & 0 \\ -j^2 & 0 & 0 & 0 \end{pmatrix}}_V. \quad (B4)$$

Details of the calculation are not presented for the sake of brevity, and finally we obtain that the effect of the mass term at second order on the low energy states of graphene in the $\{\frac{j^2|A_1, \mathbf{K}\rangle + |A_2, \mathbf{K}\rangle}{2}, \frac{j^2|B_1, \mathbf{K}\rangle + |B_2, \mathbf{K}\rangle}{2}, \frac{j|A_1, -\mathbf{K}\rangle + |A_2, -\mathbf{K}\rangle}{2}, \frac{j|B_1, -\mathbf{K}\rangle + |B_2, -\mathbf{K}\rangle}{2}\}$ basis is :

$$H^{(2)} = \begin{pmatrix} 0 & 0 & 0 & \kappa^* \\ 0 & 0 & \kappa^* & 0 \\ 0 & \kappa & 0 & 0 \\ \kappa & 0 & 0 & 0 \end{pmatrix} = (\Re(\kappa)\sigma_x + \Im(\kappa)\sigma_y)\tau_x, \quad (B5)$$

where

$$\kappa = \frac{16m^2}{N_x^2} \sum_{p \in \mathbb{Z}} \frac{1}{(1 - e^{2i\pi \frac{2p+1}{N_x}})(j - e^{-2i\pi \frac{2p+1}{N_x}})} \frac{1}{v_x(2p+1)},$$

$$v_x = \frac{\sqrt{3}\pi}{N_x}. \quad (\text{B6})$$

This Hamiltonian opens a $2|\kappa|$ gap. To compute κ we use that $N_x \rightarrow +\infty$, hence

$$\kappa \approx \frac{16m^2}{N_x^2} \sum_{p \in \mathbb{Z}} \frac{1}{2i\pi \frac{2p+1}{N_x}(1 - j - 2i\pi \frac{2p+1}{N_x})} \frac{1}{v_x(2p+1)}. \quad (\text{B7})$$

Since v_x is in $\frac{1}{N_x}$ it is justified to only keep the first order contribution in $\frac{p}{N_x}$, which will lead to a constant term thanks to the prefactor $\frac{1}{N_x^2}$, while higher order contributions will disappear in the thermodynamic limit. We get

$$\kappa \approx \frac{16m^2}{(1-j)N_x^2} \sum_{p \in \mathbb{Z}} \frac{N_x^2}{2\sqrt{3}i\pi^2(2p+1)^2} \quad (\text{B8})$$

$$= \frac{8m^2}{i(1-j)\sqrt{3}\pi^2} \sum_{p \in \mathbb{Z}} \frac{1}{(2p+1)^2} = \frac{8m^2}{i(1-j)\sqrt{3}\pi^2} 2\frac{\pi^2}{8}$$

$$= -\frac{2m^2}{\sqrt{3}(1-j)}i, \quad (\text{B9})$$

and finally

$$|\kappa| = \frac{2m^2}{3}, \quad (\text{B10})$$

which is the expression quoted in the main text. The predicted gap of $2|\kappa|$ is compared to the gap in modes we obtain by numerical exact diagonalization of the tight-binding Hamiltonian (Fig. 3d).

Finally if we go from a sharp domain wall to a smooth domain wall, the gap gets drastically reduced, as can be seen in Fig. 6. Our smooth domain walls are obtained by convolution of a sharp DW (step function) with a gaussian of desired width ξ . The drop in the value of the gap is coherent with our analysis as the value of the gap is tuned by the Fourier coefficients linking states close to K to states close to $-K$. Indeed, as the smoothness of the domain wall increases, which means as its typical width increases, the width of its Fourier transform decreases. This gives support to our assessment that the gap is a second order effect caused by the sharpness of the domain wall.

[1] A. Avsar, J. Y. Tan, T. Taychatanapat, J. Balakrishnan, G. K. W. Koon, Y. Yeo, J. Lahiri, A. Carvalho, A. S. Rodin, E. C. T. O'Farrell, G. Eda, A. H. Castro Neto, and B. Özyilmaz, Spin-orbit proximity effect in graphene, *Nature Communications* **5**, 4875 (2014).

[2] S. Zihlmann, A. W. Cummings, J. H. Garcia, M. Kedves, K. Watanabe, T. Taniguchi, C. Schönenberger, and P. Makk, Large spin relaxation anisotropy and valley-zeeman spin-orbit coupling in ws₂/graphene/h-bn heterostructures, *Phys. Rev. B* **97**, 075434 (2018).

[3] T. Wakamura, F. Reale, P. Palczynski, M. Q. Zhao, A. T. C. Johnson, S. Guéron, C. Mattevi, A. Ouerghi, and H. Bouchiat, Spin-orbit interaction induced in graphene by transition metal dichalcogenides, *Phys. Rev. B* **99**, 245402 (2019).

[4] S. Huang, K. Kim, D. K. Efimkin, T. Lovorn, T. Taniguchi, K. Watanabe, A. H. MacDonald, E. Tutuc, and B. J. LeRoy, Topologically protected helical states in minimally twisted bilayer graphene, *Phys. Rev. Lett.* **121**, 037702 (2018).

[5] P. Rickhaus, J. Wallbank, S. Slizovskiy, R. Pisoni, H. Overweg, Y. Lee, M. Eich, M.-H. Liu, K. Watanabe, T. Taniguchi, T. Ihn, and K. Ensslin, Transport through a network of topological channels in twisted bilayer graphene, *Nano Letters* **18**, 6725 (2018).

[6] H. Yoo, R. Engelke, S. Carr, S. Fang, K. Zhang, P. Cazeaux, S. H. Sung, R. Hovden, A. W. Tsien, T. Taniguchi, K. Watanabe, G.-C. Yi, M. Kim, M. Luskin, E. B. Tadmor, E. Kaxiras, and P. Kim, Atomic and electronic reconstruction at the van der waals interface in twisted bilayer graphene, *Nature Materials* **18**, 448 (2019).

[7] I. V. Lebedeva and A. M. Popov, Energetics and structure of domain wall networks in minimally twisted bilayer graphene under strain, *The Journal of Physical Chemistry C* **124**, 2120 (2020).

[8] B. Yang, M.-F. Tu, J. Kim, Y. Wu, H. Wang, J. Alicea, R. Wu, M. Bockrath, and J. Shi, Tunable spin-orbit coupling and symmetry-protected edge states in graphene/ws₂, *2D Materials* **3**, 031012 (2016).

[9] A. David, P. Rakyta, A. Kormányos, and G. Burkard, Induced spin-orbit coupling in twisted graphene-transition metal dichalcogenide heterobilayers: Twistrionics meets spintronics, *Phys. Rev. B* **100**, 085412 (2019).

[10] Y. Li and M. Koshino, Twist-angle dependence of the proximity spin-orbit coupling in graphene on transition-metal dichalcogenides, *Phys. Rev. B* **99**, 075438 (2019).

[11] I. Martin, Y. M. Blanter, and A. F. Morpurgo, Topological confinement in bilayer graphene, *Phys. Rev. Lett.* **100**, 036804 (2008).

[12] A. Vaezi, Y. Liang, D. H. Ngai, L. Yang, and E.-A. Kim, Topological edge states at a tilt boundary in gated multilayer graphene, *Phys. Rev. X* **3**, 021018 (2013).

[13] L.-J. Yin, H. Jiang, J.-B. Qiao, and L. He, Direct imaging of topological edge states at a bilayer graphene domain wall, *Nature Communications* **7**, 11760 (2016).

[14] W. Yao, S. A. Yang, and Q. Niu, Edge states in graphene: From gapped flat-band to gapless chiral modes, *Phys.*

Rev. Lett. **102**, 096801 (2009).

[15] G. W. Semenoff, V. Semenoff, and F. Zhou, Domain walls in gapped graphene, Phys. Rev. Lett. **101**, 087204 (2008).

[16] K.-I. Sasaki, R. Saito, M. S. Dresselhaus, K. Wakabayashi, and T. Enoki, Soliton trap in strained graphene nanoribbons, New Journal of Physics **12**, 103015 (2010).

[17] S.-R. E. Yang, Soliton fractional charges in graphene nanoribbon and polyacetylene: Similarities and differences, Nanomaterials **9**, 10.3390/nano9060885 (2019).

[18] P. San-Jose and E. Prada, Helical networks in twisted bilayer graphene under interlayer bias, Phys. Rev. B **88**, 121408 (2013).

[19] D. K. Efimkin and A. H. MacDonald, Helical network model for twisted bilayer graphene, Phys. Rev. B **98**, 035404 (2018).

[20] Y. H. Kwan, G. Wagner, N. Chakraborty, S. H. Simon, and S. A. Parameswaran, Domain wall competition in the chern insulating regime of twisted bilayer graphene (2020), arXiv:2007.07903 [cond-mat.str-el].

[21] O. Shevtsov, P. Carmier, C. Petitjean, C. Groth, D. Carpentier, and X. Waintal, Graphene-based heterojunction between two topological insulators, Phys. Rev. X **2**, 031004 (2012).

[22] T. Frank, P. Högl, M. Gmitra, D. Kochan, and J. Fabian, Protected pseudohelical edge states in F_2 -trivial proximitized graphene, Phys. Rev. Lett. **120**, 156402 (2018).

[23] D. Kochan, S. Irmer, and J. Fabian, Model spin-orbit coupling hamiltonians for graphene systems, Phys. Rev. B **95**, 165415 (2017).

[24] L. Razzaghi and M. V. Hosseini, Quantum transport of dirac fermions in graphene with a spatially varying rashba spin-orbit coupling, Physica E: Low-dimensional Systems and Nanostructures **72**, 89 (2015).

[25] A. Brataas, A. G. Mal'shukov, and Y. Tserkovnyak, Spin injection in quantum wells with spatially dependent rashba interaction, New Journal of Physics **9**, 345 (2007).

[26] J. Teo and C. Kane, Topological defects and gapless modes in insulators and superconductors, Physical Review B **82**, 115120 (2010).

[27] C.-K. Chiu, J. C. Y. Teo, A. P. Schnyder, and S. Ryu, Classification of topological quantum matter with symmetries, Reviews of Modern Physics **88**, 035005 (2016).

[28] E. Prodan, Non-commutative tools for topological insulators, New Journal of Physics **12**, 5003 (2010).

[29] E. Prodan, Robustness of the spin-Chern number, Physical Review B **80**, 125327 (2009).

[30] D. N. Sheng, Z. Y. Weng, L. Sheng, and F. D. M. Haldane, Quantum spin-hall effect and topologically invariant chern numbers, Phys. Rev. Lett. **97**, 036808 (2006).

[31] M. Ezawa, Topological kirchhoff law and bulk-edge correspondence for valley chern and spin-valley chern numbers, Phys. Rev. B **88**, 161406 (2013).

[32] M. Ezawa, Spin valleytronics in silicene: Quantum spin hall-quantum anomalous hall insulators and single-valley semimetals, Phys. Rev. B **87**, 155415 (2013).

[33] T. T. Heikkilä, N. B. Kopnin, and G. E. Volovik, Flat bands in topological media, JETP Letters **94**, 233 (2011).

[34] F. Faure, Manifestation of the topological index formula in quantum waves and geophysical waves (2019), arXiv:1901.10592 [math-ph].

[35] M. Marciani and P. Delplace, Chiral maxwell waves in continuous media from berry monopoles, Phys. Rev. A **101**, 023827 (2020).

[36] A. M. Alsharari, M. M. Asmar, and S. E. Ulloa, Mass inversion in graphene by proximity to dichalcogenide monolayer, Phys. Rev. B **94**, 241106 (2016).

[37] J. Klinovaja, G. J. Ferreira, and D. Loss, Helical states in curved bilayer graphene, Phys. Rev. B **86**, 235416 (2012).

[38] A. Inhofer, S. Tchoumakov, B. A. Assaf, G. Fève, J. M. Berroir, V. Jouffrey, D. Carpentier, M. O. Goerbig, B. Plaçais, K. Bendias, D. M. Mahler, E. Bocquillon, R. Schlereth, C. Brüne, H. Buhmann, and L. W. Molenkamp, Observation of volkov-pankratov states in topological hgte heterojunctions using high-frequency compressibility, Phys. Rev. B **96**, 195104 (2017).

[39] B. Braunecker and P. Simon, Interplay between classical magnetic moments and superconductivity in quantum one-dimensional conductors: Toward a self-sustained topological majorana phase, Phys. Rev. Lett. **111**, 147202 (2013).

[40] B. Tsim, N. N. T. Nam, and M. Koshino, Perfect one-dimensional chiral states in biased twisted bilayer graphene, Phys. Rev. B **101**, 125409 (2020).

[41] J. D. Sau, S. Tewari, R. M. Lutchyn, T. D. Stanescu, and S. Das Sarma, Non-Abelian quantum order in spin-orbit-coupled semiconductors: Search for topological Majorana particles in solid-state systems, Physical Review B **82**, 214509 (2010).

[42] G. C. Ménard, A. Mesaros, C. Brun, F. Debontridder, D. Roditchev, P. Simon, and T. Cren, Isolated pairs of Majorana zero modes in a disordered superconducting lead monolayer, Nature Communications **10**, 1 (2019).